Electronic Supplementary Information:

Effect of Different Halide-Based Ligands on the Passivation and Charge Carrier Dynamics in $AgBiS_2$ Nanocrystal Solar Cells

Fiona Treber[a], Elke De Grande[a], Ute B. Cappel[b,c], Erik M. J. Johansson*[a]

[a] Department of Chemistry-Ångström, Physical Chemistry, Uppsala University, 75120 Uppsala, Sweden.

[b] Condensed Matter Physics of Energy Materials, Division of X-ray Photon Science, Department of Physics and Astronomy, Uppsala University, 75120 Uppsala, Sweden.

[c] Wallenberg Initiative Materials Science for Sustainability, Department of Physics and Astronomy, Uppsala University, 75120 Uppsala, Sweden.

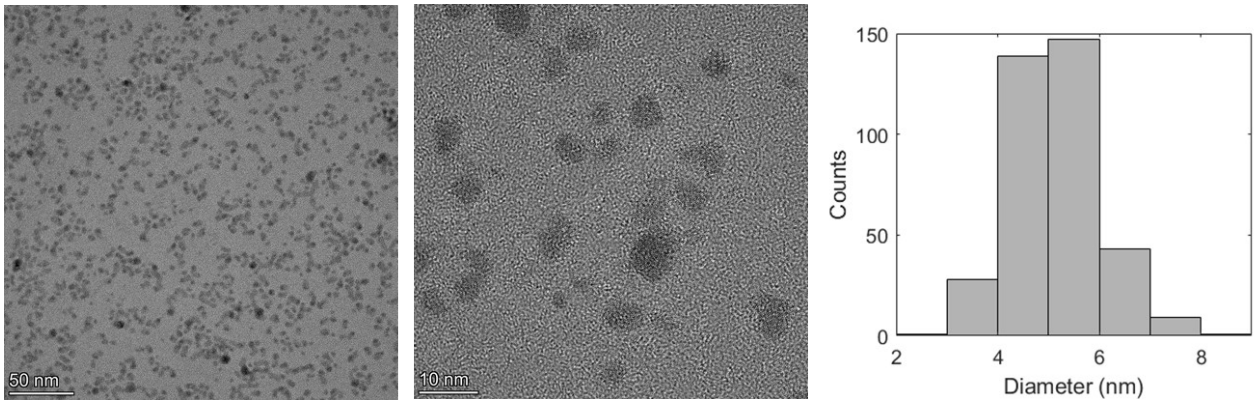

Figure S1: Additional TEM images of the as-synthesised $AgBiS_2$ NCs and resulting size distribution histogram.

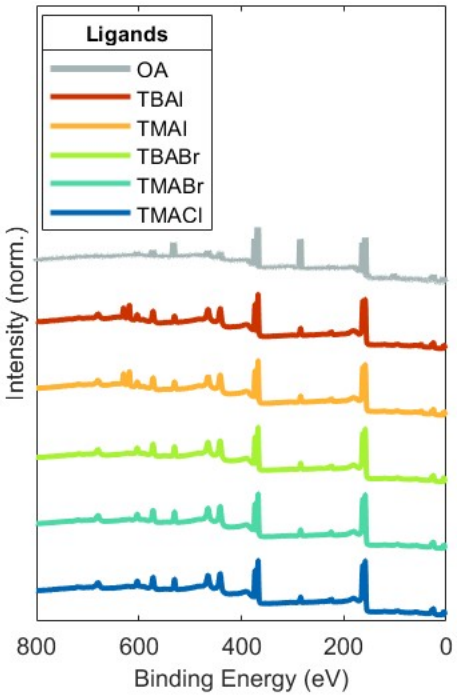

Figure S2: XPS survey spectra of the five ligand-exchanged thin films (TBAI, TMAI, TBABr, TMABr, TMACl), as well as the corresponding spectrum from the as-synthesised NCs (denoted by OA) passivated with the long-chain aliphatic ligands.

Table S1: Relative elemental contribution from carbon and oxygen to the overall impurity/surface contamination signal. The elemental ratio between impurities/surface contamination and the $AgBiS_2$-nanocrystal-related constituents is about 1:1 for all ligand-exchanged samples (TBAI, TMAI, TBABr, TMABr, TMACl). For the as-synthesised NCs (denoted by OA) passivated with the long-chain aliphatic ligands, this ratio it is 4:1 instead, signifying a much higher amount of oxygen and carbon present in the sample, as expected.

	OA	TBAI	TMAI	TBABr	TMABr	TMACl
C (%)	82	75	69	61	63	60
O (%)	18	25	31	39	37	40

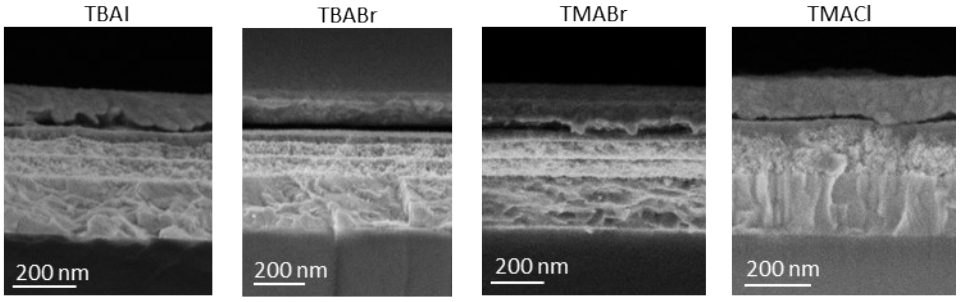

Figure S3: SEM cross-section images of the remaining 4 solar cell samples.

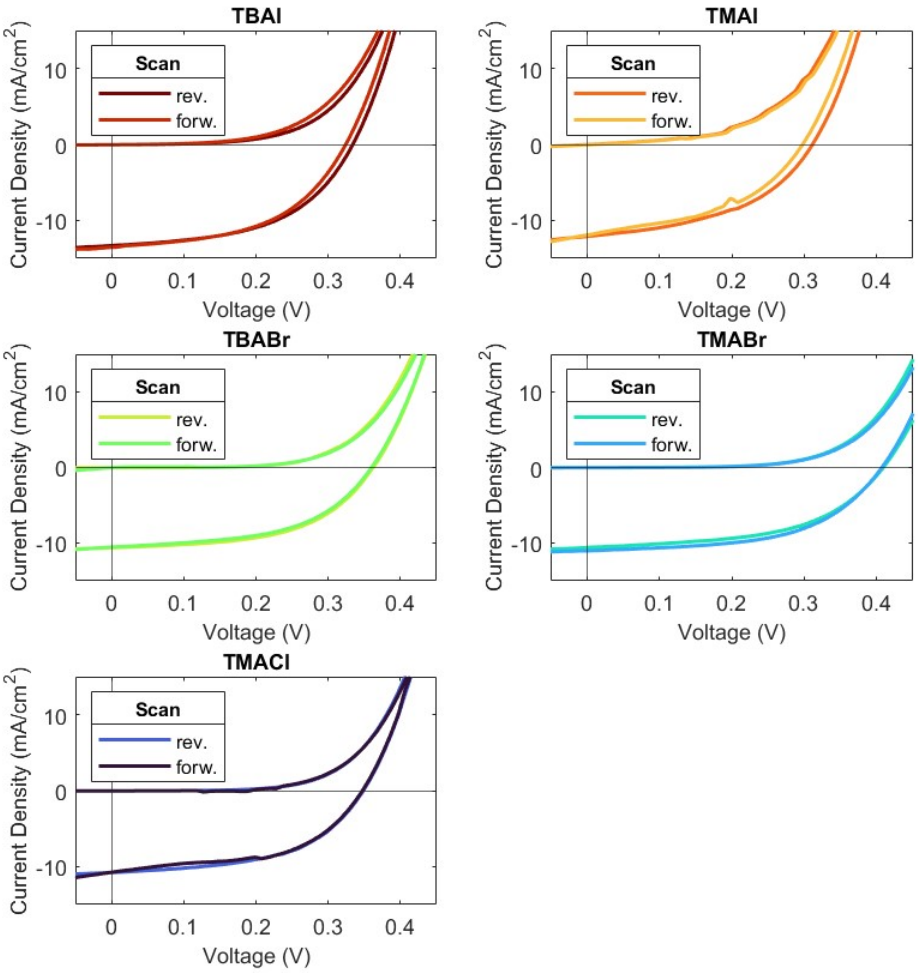

Figure S4: JV curves measured in reverse and forward direction with no significant hysteresis visible, both under 1 sun illumination, as well as in the dark.

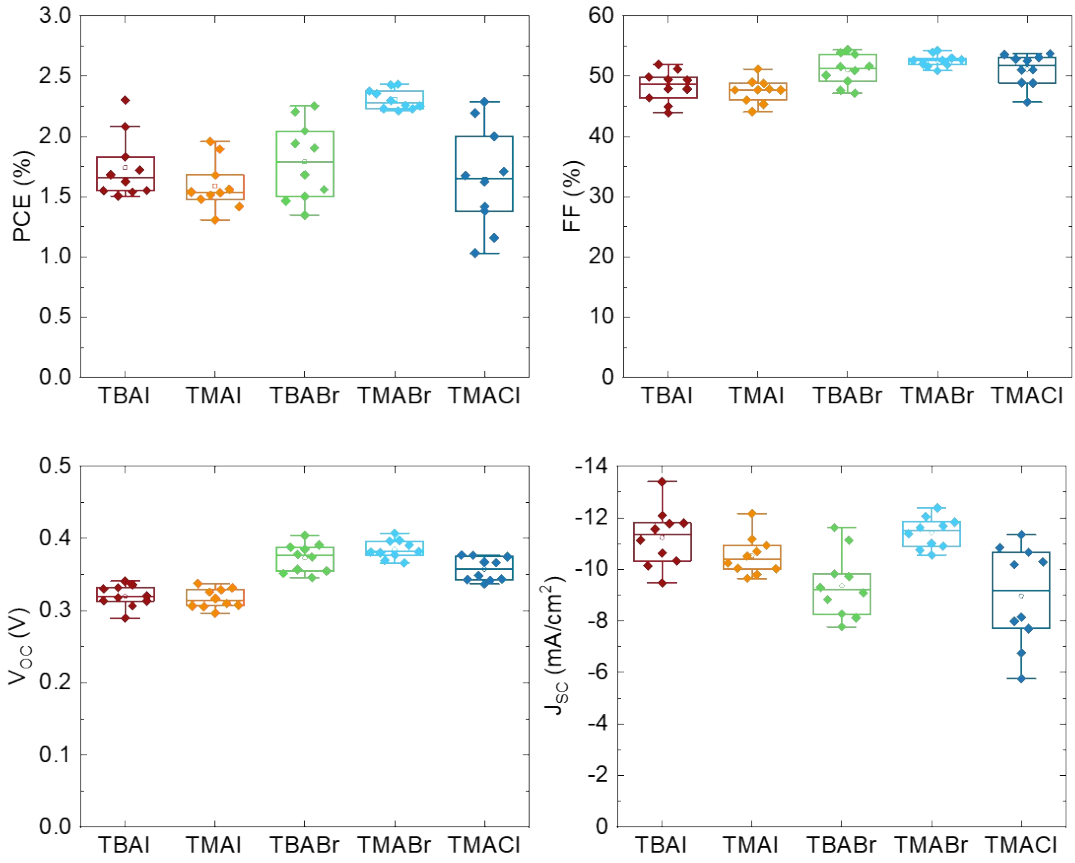

Figure S5: Box plots of PCE, FF, Jsc and Voc for 10 devices made with each respective ligand passivation. Measurements were carried out under 1 sun illumination.

Table S2: Integrated J_{SC} from IPCE measurements.

	TBAI	TMAI	TBABr	TMABr	TMACl
J_{SC} (mA/cm^2)	12.04	11.92	9.93	9.67	9.21

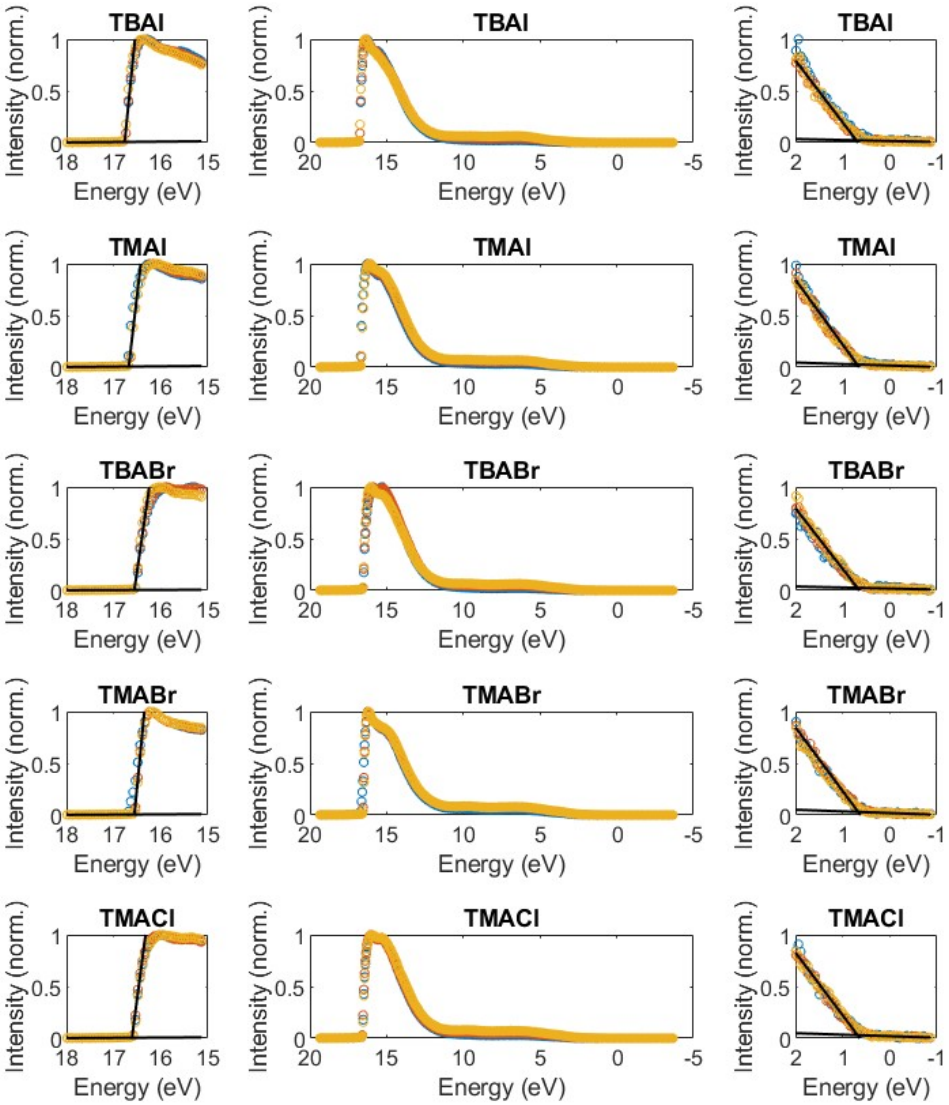

Figure S6: UPS data for each sample with linear fits (black) to determine the cut-off and the valence band maximum (VBM) vs. the Fermi level. 3 consecutive measurements are depicted in each case (blue, red and yellow markers) to test for stability of result.

Table S3: Position of the work function (WF), as well as the valence band maximum (VBM) relative to the Fermi level (E_F), as extracted from UPS data.

	TBAI	TMAI	TBABr	TMABr	TMACl
WF (eV)	-4.45	-4.54	-4.66	-4.66	-4.61
VBM vs. E_F (eV)	-0.71	-0.69	-0.69	-0.67	-0.68

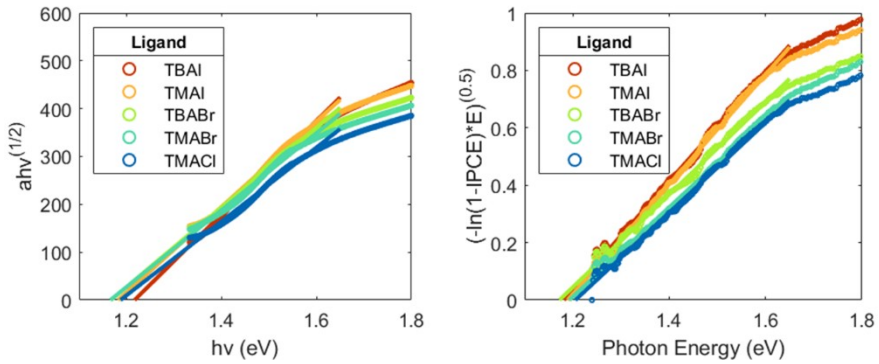

Figure S7: Tauc plot from absorbance data of thin films (left) and equivalent band gap estimation from IPCE data (right).

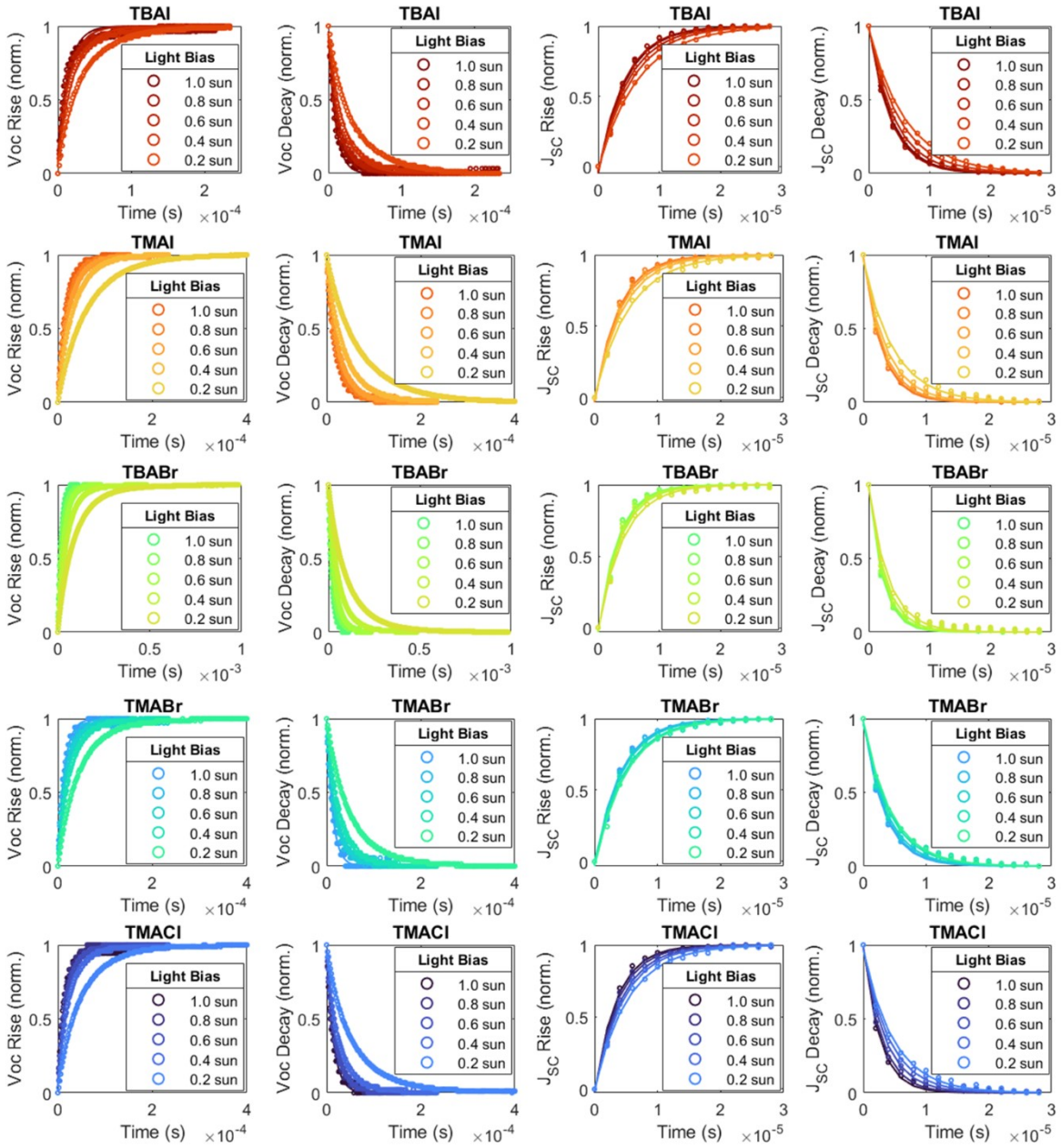

Figure S8: Data and fits from TPV/TPJ measurements (Voc and Jsc Rise/Decay; single exponential fit) for all five ligand-exchanged samples under varying light bias.

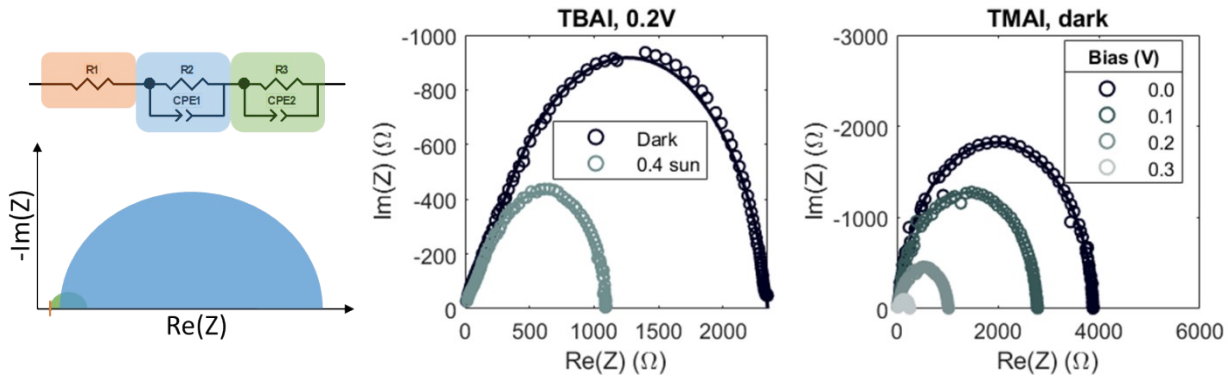

Figure S9: Impedance data examples and equivalent circuit. Left: Model/equivalent circuit used to fit all impedance data presented here, comprised of a series resistance resulting in a small offset along the x-axis (red) and two RQ-elements corresponding to the smaller (green) and larger (blue) semicircle in the schematic illustration underneath. Middle: Differences due to illumination (example: TBAI at 0.2 V). Right: Trend with increasing forward bias (example: TMAI, dark).

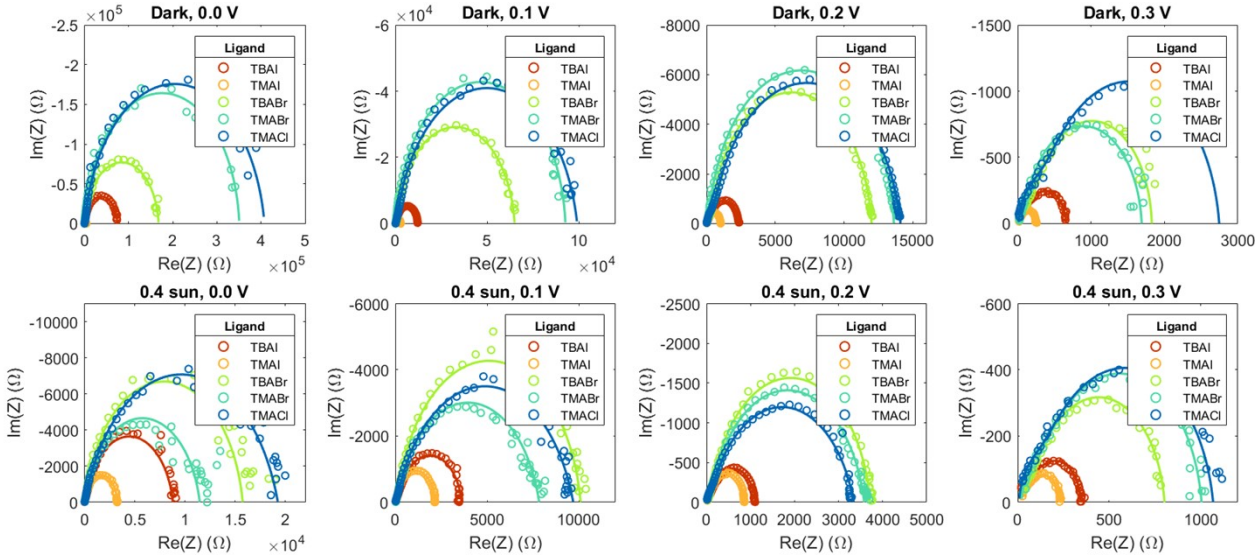

Figure S10: Impedance data and fits, according to equivalent circuit shown in Fig. S9, for all samples and measurement conditions (offset bias: 0.0-0.3 V, illumination: dark or 0.4 sun equivalent).